Global Change Biology

WILEY

Global Change Biology

RESEARCH ARTICLE OPEN ACCESS

Recovery Following Recurrent Fires Across Mediterranean Ecosystems

Tiago Ermitão[1,2] | Célia M. Gouveia[1,2] | Ana Bastos[3,4] | Ana C. Russo[1,5]

[1]Faculdade de Ciências, Instituto Dom Luiz, Universidade de Lisboa, Lisbon, Portugal | [2]Instituto Português do Mar e da Atmosfera, IPMA, Lisbon, Portugal | [3]Department of Biogeochemical Integration, Max Planck Institute for Biogeochemistry, Jena, Germany | [4]Institute for Earth System Science and Remote Sensing, Leipzig University, Leipzig, Germany | [5]Associate Laboratory TERRA, CEF – Forest Research Centre, School of Agriculture, University of Lisbon, Lisboa, Portugal

Correspondence: Tiago Ermitão (tmrsilva@ciencias.ulisboa.pt)

Received: 12 August 2024 | **Accepted:** 6 December 2024

Funding: This study was performed under the framework of the DHEFEUS project, funded by Fundação para a Ciência e a Tecnologia (FCT) (https://doi.org/10.54499/2022.09185.PTDC). A.C.R. is supported by the FCT through national funds from the MCTES within the Faculty of Sciences of the University of Lisbon, through https://doi.org/10.54499/2022.01167.CEECIND/CP1722/CT0006. A.B. acknowledges funding by the European Union (ERC StG, ForExD, grant agreement No. 101039567). T.E. was supported by the doctoral Grant PRT/BD/154296/2022 financed by the Portuguese FCT under the MIT Portugal Program.

Keywords: climate variability | EVI | fire severity | post-fire recovery | pre-fire vegetation conditions | remote-sensing

ABSTRACT

In fire-prone regions such as the Mediterranean biome, fire seasons are becoming longer, and fires are becoming more frequent and severe. Post-fire recovery dynamics is a key component of ecosystem resilience and stability. Even though Mediterranean ecosystems can tolerate high exposure to extreme temperatures and recover from fire, changes in climate conditions and fire intensity or frequency might contribute to loss of ecosystem resilience and increase the potential for irreversible changes in vegetation communities. In this study, we assess the recovery rates of burned vegetation after recurrent fires across Mediterranean regions globally, based on remotely sensed Enhanced Vegetation Index (EVI) data, a proxy for vegetation status, from 2001 to 2022. Recovery rates are quantified through a statistical model of EVI time-series. This approach allows resolving recovery dynamics in time and space, overcoming the limitations of space-for-time approaches typically used to study recovery dynamics through remote sensing. We focus on pixels burning repeatedly over the study period and evaluate how fire severity, pre-fire vegetation greenness, and post-fire climate conditions modulate vegetation recovery rates of different vegetation types. We detect large contrasts between recovery rates, mostly explained by regional differences in vegetation type. Particularly, needle-leaved forests tend to recover faster following the second event, contrasting with shrublands that tend to recover faster from the first event. Our results also show that fire severity can promote a faster recovery across forested ecosystems. An important modulating role of pre-fire fuel conditions on fire severity is also detected, with pixels with higher EVI before the fire resulting in stronger relative greenness loss. In addition, post-fire climate conditions, particularly air temperature and precipitation, were found to modulate recovery speed across all regions, highlighting how direct impacts of fire can compound with impacts from climate anomalies in time and likely destabilise ecosystems under changing climate conditions.

1 | Introduction

Warmer and drier climate conditions in the past decades have been changing fire regimes (Pausas and Keeley 2021; Scholten et al. 2021; Jones et al. 2022, 2024), with extreme events associated with unprecedented fires in many ecosystems worldwide (Scholten et al. 2021; Byrne et al. 2024; Jones et al. 2024). These have been particularly evident in semi-arid areas across the globe, such as the Mediterranean regions. For instance, in Europe, severe fire seasons in 2003, 2017 and 2022 occurred in Portugal and Spain (Gouveia et al. 2012; Turco et al. 2019; Ermitão et al. 2022, 2023; Ramos et al. 2023; Rodrigues et al. 2023), and in Greece and southern Italy during 2007, 2021, and 2023 (Gouveia et al. 2016; Evelpidou et al. 2021; Dosiou et al. 2024). Destructive wildfires also occurred in California in 2018, 2020 and 2021 (Brown et al. 2020; Higuera and Abatzoglou 2021), in Chile in 2017 and more recently in 2023 and 2024 (McWethy et al. 2018; Bowman et al. 2019; Cordero et al. 2024), in South Africa in 2021 (Liu et al. 2023) and in Australia, both in Mediterranean-type ecosystems in 2015 (Etchells et al. 2020) and non-Mediterranean-type vegetation in 2006–2007 and 2019–2020 (McCarthy, Plucinski, and Gould 2012; Filkov et al. 2020).

Mediterranean ecosystems tend to experience frequent fires, with return intervals shorter than 20 years (Archibald et al. 2013; Harrison et al. 2021) and plants often exhibit fire adaptations such as thick barks, resprouting ability, or stimulation of reproduction after fire exposure (Lawes and Clarke 2011; Clarke et al. 2013; Pausas 2015; Harrison et al. 2021; Nolan et al. 2021). However, increasing frequency and severity of weather and climate extremes (Zscheischler et al. 2018; Vogel et al. 2021) can result in repeated impacts on ecosystems, so that their recovery might be limited (Davis, Shaw, and Etterson 2005; Brito-Morales et al. 2018; Bastos et al. 2020, 2021). Compound effects of repeated weather extremes and changes in disturbance regimes can thus increase the potential for irreversible changes in ecological communities (Seidl and Turner 2022; Bastos et al. 2023). Therefore, the effects of recurrent extremes on ecosystem resilience have been gaining increasing attention (Anderegg, Kane, and Anderegg 2013; Falk, Watts, and Thode 2019; Steel et al. 2021; Bastos et al. 2021).

Ecological resilience can be decomposed into three different stages (Falk et al. 2022): *persistence*, the ability to tolerate exposure to the fire, *recovery*, which occurs when *persistence* is overcome and the vegetation must recover by reproduction e.g., recruitment, seed dispersal, and *reorganisation*, that occurs when *persistence* and *recovery* fail, and the ecosystem reorganises into a new state. While recovery dynamics is central to understanding ecosystem resilience, it is a complex process, being controlled by multiple factors such as disturbance impacts and climate (Meng et al. 2018; Bright et al. 2019; Nolan et al. 2021), but also land cover (Díaz-Delgado et al. 2002; Epting and Verbyla 2005), topography (Wittenberg et al. 2007; Meng et al. 2015; Liu 2016) or the distance to seed banks (Donato et al. 2009). Moreover, human intervention and soil and land management after fire can modulate recovery dynamics (Baeza et al. 2007; Vieira et al. 2023).

Remote sensing has been widely used to study fire impacts and recovery dynamics (Díaz-Delgado and Pons 2001; Díaz-Delgado et al. 2002; Wittenberg et al. 2007; Gouveia, DaCamara, and Trigo 2010; Gouveia et al. 2012; Gouveia, Páscoa, and DaCamara 2018; Bastos et al. 2011; De Luca, Silva, and Modica 2022) as well as the influence of post-fire climate conditions, topography or fire severity in some regions (Díaz-Delgado et al. 2002; Liu 2016; Viana-Soto, Aguado, and Martínez 2017). Regional studies have pinpointed the synergy between fire severity, pre-fire vegetation state, and climate conditions on vegetation recovery: Bright et al. (2019) in western USA, Viana-Soto et al. (2020) in Spain, and Rifai et al. (2024) in Australia. At a larger scale, Bousquet et al. (2022) analysed the recovery of different ecosystems worldwide after a fire event, by comparing different vegetation-related variables such as Enhanced Vegetation Index (EVI), Leaf Area Index (LAI), and aboveground biomass (AGB). Analysis of recovery dynamics at larger scales typically relies on space-for-time substitution approach, assuming the stationarity of recovery dynamics following fire events, and cannot resolve changes in recovery dynamics, e.g., due to varying climate conditions during the recovery periods, not temporally compounding effects of recurring fires (Moreno-Mateos et al. 2020).

So far, no comprehensive assessment of recovery dynamics across space and time, including the effects of climate variability during the process has been performed for a broader region. Such information is especially relevant in regions recurrently disturbed by fires and exposed to climate change effects, such as the Mediterranean biome. Therefore, we provide a first comprehensive analysis of recovery dynamics of vegetation following recurrent fires over Mediterranean ecosystems worldwide based on a remotely sensed proxy for vegetation cover, the EVI over the period 2001–2022. With this approach, we also aim to evaluate how vegetation recovery is modulated by fire severity, pre-fire state of vegetation, and post-fire meteorological conditions. This framework intends to address the main scientific questions: (i) are the recovery processes of fire-prone Mediterranean ecosystems being impacted by recurrent fires in recent years? (ii) how does the pre-fire condition of these ecosystems influence fire severity, and in turn, how does fire severity modulate the recovery rate of burned vegetation? (iii) how can post-fire meteorological conditions affect the recovery rate among the Mediterranean ecosystems worldwide?

2 | Data

2.1 | Biome

We use the definition of Mediterranean biome by Dinerstein et al. (2017), which is an updated version of the original biome map of 2001 by Olson et al. (2001). The dataset by Dinerstein et al. (2017) provides updated information of the 846 global ecoregions, nested within the 14 global biomes, where each one is defined based on homogeneous climate and vegetation characteristics.

2.2 | Burned Area

To analyse the occurrence of fires over global Mediterranean ecosystems, we use monthly burned area and burn date uncertainty

maps in each fire season from MODIS version 6.1, MCD64A1 (Giglio et al. 2018) between 2001 and 2022. The data have a spatial resolution of 500 m in its native projection and are generated using daily surface reflectance dynamics and thermal anomalies, allowing the detection of the most likely fire date. Several improvements to the algorithm have been integrated into the latest collection, especially regarding small fire detection and also the reduction of uncertainty on burn-date guessing.

Data used here were extracted for the seasonal extended fire seasons, according to information provided in the Global Wildfire Information System (GWIS) Portal (https://gwis.jrc.ec.europa.eu/apps/country.profile/, accessed on 30 June 2023) in each of the five selected regions: in the Mediterranean basin and California, the typical fire seasons extend from June to October, in Australia between October and February while in South Africa and Chile extend from December to April.

2.3 | Vegetation Indices

EVI quantifies the greenness of the land surface and provides a proxy for vegetation cover and condition, including several adjustments regarding the canopy background and atmospheric corrections and showing lower saturation over high-density canopies compared to other vegetation spectral indices (Huete et al. 2002; Didan et al. 2015; Xu et al. 2020). Therefore, EVI is a suitable index to assess the recovery of vegetation after disturbances due to its strong sensitivity to seasonal or biophysical changes (Wittenberg et al. 2007; Veraverbeke et al. 2012; Pérez-Cabello, Montorio, and Alves 2021).

Here, we use EVI from MODIS Collection 6.1 (MOD13A1, Didan et al. (2015)) to monitor vegetation dynamics, fire severity, and recovery. MODIS EVI is provided as 16-day composites at a spatial resolution of 500 m in its native projection. For our study, we extracted the EVI between 2001 and 2022, to match the period available for burned areas.

2.4 | Land Cover

The land-cover distribution analysis over the Mediterranean biome is based on the land-cover product from ESA CCI Land Cover, CCI-LC (Kirches et al. 2014), which provides global land cover at a spatial resolution of 300 m and is available between 1992 and 2020. By combining global surface reflectance data from five different Earth Observation systems (Liu et al. 2018), the product describes the surface cover in 37 original LC classes following the United Nations Land Cover Classification System (UN-LCCS, Di Gregorio 2005; Liu et al. 2018). For our work, the annual maps for the period 2001–2020 were extracted. Considering that CCI-LC is available up to 2020, we used the 2020 land-cover classification map for 2021 and 2022.

2.5 | Climate Data

We use precipitation and 2 m air temperature data from the ERA5-Land reanalysis at 9 km (0.10°) spatial resolution, available since 1950 (Muñoz-Sabater et al. 2021). ERA5-Land is a downscale product based on ERA5 and shows strong performance on energy and hydrological cycle modulation, with higher spatial resolution and longer temporal coverage (Muñoz-Sabater et al. 2021), allowing us to better characterise the post-fire meteorological conditions in our study. The meteorological variables, such as precipitation and 2 m air temperature from ERA5-Land, have been recently used to characterise the recovery of burned vegetation, for example, in Spain (Rodrigues et al. 2023) or in Australia (Rifai et al. 2024). In our study, we selected the period 2001–2022 to match the period selected for vegetation and burned areas data.

3 | Methods

3.1 | Study Region

We analysed fire recurrence over five Mediterranean regions across the globe: the Mediterranean basin, southern California, southwestern and southern Australia, southwestern South Africa, and along the coast of Chile (Figure 1, top panel). These regions usually have wet and mild to cool autumn and winter seasons, whereas the summers are characterised by hot and dry conditions (Figure S1), being essentially classified as *Csa* and *Csb* in the Köppen-Geiger classification (Köppen 1936). The land-cover distribution in these regions is heterogeneous (see Figure 1 for land-cover distribution in regions within the Mediterranean biome). Needleleaf trees (*NL*) are predominant in California and the Mediterranean basin, especially in the Iberian Peninsula, while broad-leaved trees (*BL*) are present in all regions except California, predominating in several areas of western Australia and parts of northern Africa near the coast. In turn, transitional woodland vegetation (*TW*) is mainly present in the Mediterranean basin, while shrublands (*Shb*) cover all regions, especially in South Africa or California.

3.2 | Data Pre-Processing

For the 16-day EVI composites, the pre-processing of data followed a technique that was previously proposed by Los (1998) and Stöckli and Vidale (2004) and was successfully applied to correct the NDVI time-series from SPOT/VEGETATION by Gouveia, Trigo, and DaCamara (2009); Gouveia, DaCamara, and Trigo (2010). Low-quality pixels (contaminated by clouds, snow, ice, or other issues) were primarily replaced through spatial interpolation, and then the EVI time-series in each pixel of the composite was adjusted by using a temporal cubic interpolation procedure. Despite the quality correction, strong fluctuations in time-series at pixel-scale were still found. Therefore, an unweighted second-order Fast Fourier Transformation (FFT) was applied, aiming to remove the noise but retaining the small-scale variations, as well as the signature of disturbances in vegetation. Vegetation indexes show long-term trends, which can be due to different drivers (Zhu et al. 2016), and such long-term trends would influence the estimate of recovery times, especially when comparing recurrent events within a time-series with 20 years long. Therefore, aiming to reduce these effects, we detrended each pixel's time-series using a locally estimated

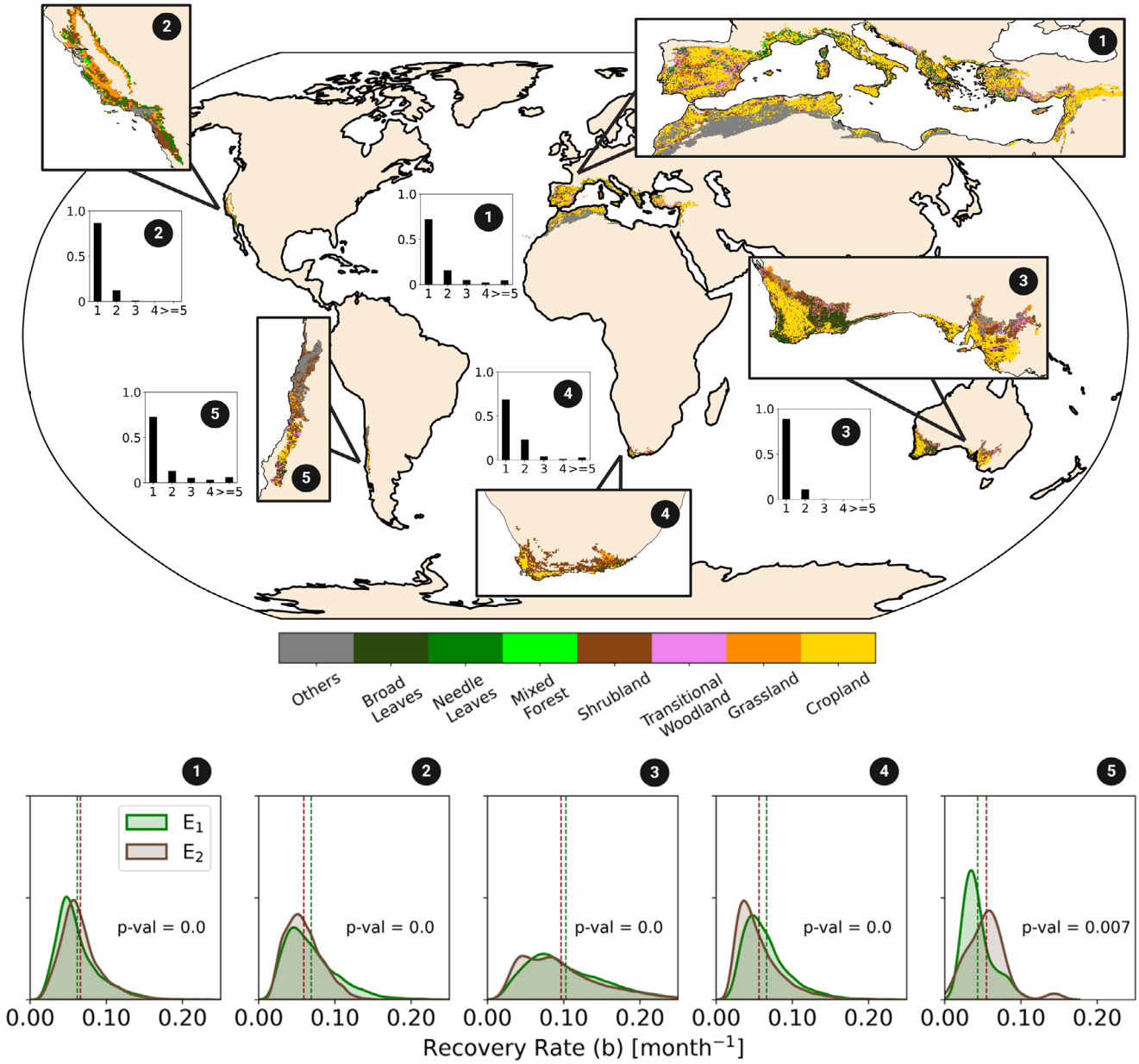

FIGURE 1 | Top panel: Global distribution of the defined categories of land cover over considering each region of the Mediterranean biome: 1—Mediterranean basin; 2—California; 3—Australia; 4—South Africa; 5—Chile. The relative fire frequency is represented on black bars for each region; Bottom panel: Probability Density Functions (PDFs) of recovery rate distribution of burned vegetation (parameter *b*, in month^{-1}) for different regions following the first fire event, E_1 (green curve) and second fire event, E_2 (brown curve). In the *y*-axis, the density of probability is represented. The p-value of the Wilcoxon signed-rank test to determine if the difference between distributions is statistically significant is represented for each region. Dashed vertical lines represent the mean recovery rate, *b*, for E_1 (green) and E_2 (brown). Map lines delineate study areas and do not necessarily depict accepted national boundaries.

scatterplot smoothing technique (LOESS technique, Cleveland et al. 1990).

Vegetation indices and climate data were aggregated into 16-day composites, re-gridded to geographical projection, and re-sampled into 0.005° latitude×0.005° longitude resolution. The annual land-cover maps were resampled to the same spatial resolution using majority resampling. We aggregated the original 37 classes of land cover from CCI-LC into seven main categories, according to different characteristics of vegetation, namely: Broad-leaved, *BL* (classes 50, 60); Needle-leaved, *NL* (classes 70, 80); Mixed Forest, *MF* (class 90); Shrubland, *Shb* (classes 40, 110, 120); Transitional Woodland, *TW* (class 100); Grassland, *Gs* (class 130); Cropland, *Cp* (classes 10, 20, 30); and Others, *Oth* (classes between 150 and 220).

3.3 | Fire Recurrence

Following the identification of the global areas classified as Mediterranean biome, we then monitored the burned areas within those ecosystems. The MCD64A1 dataset has inherent uncertainty from optical surface reflectance measurements and thermal anomalies (Brennan et al. 2019) that can introduce

additional inaccuracy in burned areas detection (Vermote, El Saleous, and Justice 2002). Thus, after a sensitivity analysis, burned pixels with an uncertainty date of burn detection longer than 7 days were excluded.

First, we quantified fire frequency between 2001 and 2022 across the whole Mediterranean biome (see Figure 1). We are interested in assessing potential changes in recovery rates over the study period. Therefore, we focus on pixels burning more than once. At the same time, the time-series is still relatively short (22 years) compared to the typical recovery periods of certain vegetation types across Mediterranean ecosystems (about 20 years, Archibald et al. 2013). For instance, Gouveia, DaCamara, and Trigo (2010); Gouveia, Páscoa, and DaCamara (2018) and Bastos et al. (2011) estimated that the NDVI of several burned areas following the fire events of 2003 and 2005 in Portugal recovered on average to pre-fire greenness levels in 3–5 years (though some areas took longer). Similarly, Viana-Soto, Aguado, and Martínez (2017) and Hislop et al. (2018) estimated 5–7 years for forests in the Iberian Peninsula to recover to pre-fire greenness levels. Lastly, Bousquet et al. (2022) reported that Australian eucalyptus took approximately 3 years to recover to pre-fire EVI levels. Therefore, as our statistical approach requires a long-enough period post-fire to estimate recovery time robustly (see sections below), we focus on pixels that burned twice over the study period, and occurred at least four years apart.

3.4 | Recovery Model

We followed the approach proposed by Gouveia, DaCamara, and Trigo (2010) to estimate post-fire recovery based on a statistical regression model of vegetation greenness following fire. First, we aggregated the 16-day composites of EVI per month and calculated, at the pixel-level, the departure of observed EVI to an ideal seasonal cycle, referred to as the Gorgeous Year, GY(t) (see Figure 2 for schematic representation). This annual vegetative cycle GY(t) is defined by estimating the highest EVI value in each monthly interval over the period 2001–2022 (Figure 2A). The normalisation of observed EVI by the GY(t) over time generates a time-series, hereafter named as $y(t)$, and defined as:

$$y(t) = \mathrm{EVI}(t) - \mathrm{GY}(t) \quad (1)$$

Therefore, $y(0)$ ranges between −1 and 0, and, the further it departs from zero, the greater the loss of greenness at a given pixel, relative to its ideal state.

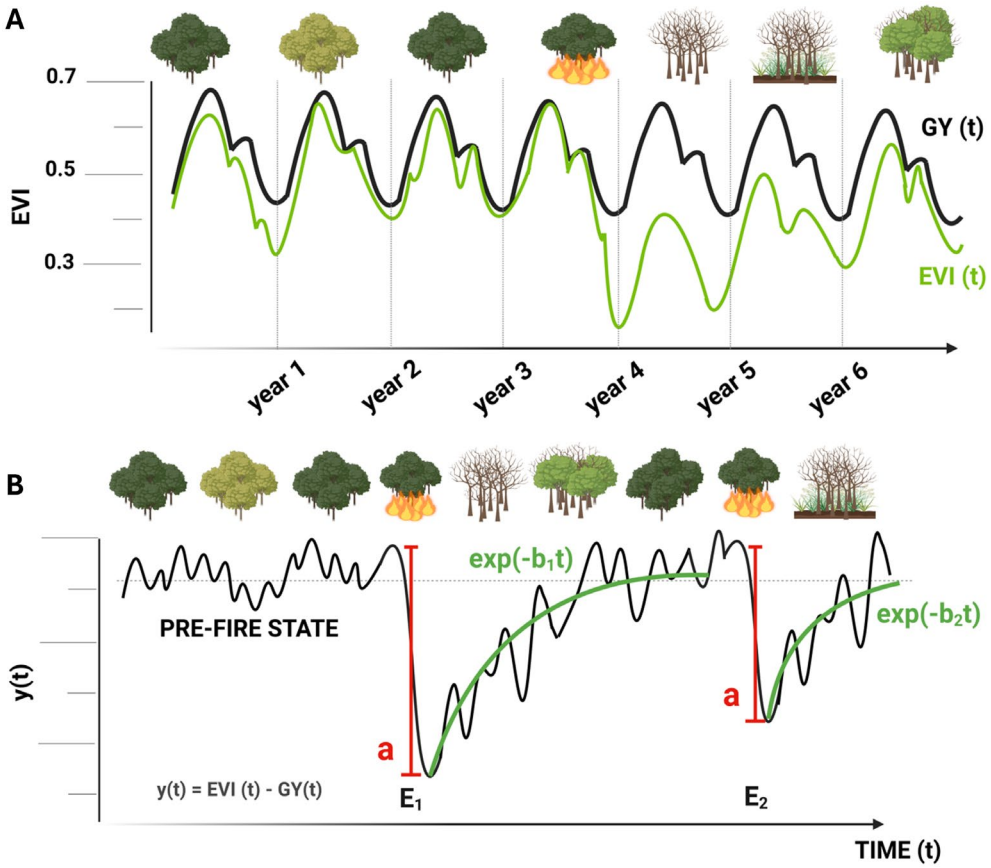

FIGURE 2 | (A) Schematic representation of the time-series of monthly EVI (green curve) and monthly GY (black curve) and the impact of a fire event in one pixel. (B) Schematic representation of the impact of two fire events in the time-series of loss of greenness, $y(t)$. The largest loss of greenness caused by fire is represented by a (red vertical lines) for the first fire event (E_1) and second fire event (E_2). The adjusted recovery model for each event is represented in green curves, and the model's equation is also described. The mean pre-fire state of the ecosystem is characterised by the black dashed line. Figure created with BioRender.com.

To estimate post-fire recovery, it is assumed that the greenness recovery rate, dy/dt, is proportional to the loss of greenness $y(t)$:

$$\frac{dy}{dt} = -by \tag{2}$$

Or, integrating:

$$y(t) = ae^{-bt} \tag{3}$$

The parameter a corresponds to the minimum of $y(t)$, i.e., the maximum loss of greenness associated with fire, whereas the parameter b expresses the recovery rate following the fire event (Figure 2B). A "characteristic recovery time" can also be derived by inverting the mean recovery rate ($1/b$), corresponding to the time in which ca. 50% of relative recovery is reached.

It is worth noting that the recovery rates estimated here correspond to the recovery of surface greenness as seen by optical remote-sensing, not necessarily the full recovery in terms of accumulated biomass and ecosystem functioning. These are expected to take longer (Bousquet et al. 2022; Fan et al. 2023).

3.5 | Model Fitting

Vegetation indexes can monitor the impact of fire events on ecosystems (Gouveia, DaCamara, and Trigo 2010; Gouveia et al. 2012; Gouveia, Páscoa, and DaCamara 2018; Bastos et al. 2011; Bright et al. 2019). However, sharp anomalies in time-series that might result from factors such as satellite-sensor drifts, human interventions, land-cover changes, or other climatic extreme events, were detected. To ensure that the loss of greenness corresponds to the impact of the fire, we estimated the minimum value of $y(t)$ between the fire occurrence and the immediate weeks after the fire event.

The recovery rate b of each pixel can be estimated by means of the slope of the linear regression applied to the $\ln(y(t))$ in the years following the occurrence of a:

$$\ln\left(\frac{y(t)}{a}\right) = -bt \tag{4}$$

The parameter b is estimated iteratively, and based on the linear regression model showing the best performance (given by the adjusted r^2), when fitting to periods of different lengths (2–5 years) following the occurrence of the minimum of $y(t)$. This iterative approach implies that different post-fire period lengths are selected for each pixel, depending on the variability of $y(t)$, but ensure that the most robust model is used. For some events, the statistical model showed poor fit to $y(t)$, hindering robust quantification of recovery rates, therefore, we excluded pixels in which both statistical model's event showed adjusted r^2 values lower than 0.25.

We analysed the results separately for the following land-cover categories: *BL*, *NL*, *Shb*, and *TW*, based on the per-pixel classification in the year before the fire event. We assumed that the land-cover category of the pixel is the same for the two events, disregarding any land-cover shifts that may happen between fires.

The selected number of points for the recovery model of each land-cover category and each region of the domain are described in Table 1.

The performance of the statistical model for E_1 and E_2, evaluated using squared regression coefficient, r^2, for each land-cover category, as well as for each fire event, is described in Figure S2. The model exhibits, for both events, a higher median performance for *NL* (r^2 of about 0.65), although with slight differences between fire events, followed by *BL* and *TW*. In *Shb*, the performance is lower, showing a median r^2 of about 0.50. Across the four land-cover categories, the r^2 distribution generally spans from 0.30 to 0.80, exhibiting some event-specific variations. The model skill also shows regional differences (map of Figure S3), with the Mediterranean basin, particularly in Portugal and northern Africa, and California showing the best model fit and some areas in South Africa showing lower values of the r^2, indicating a poorer model adjustment to the data.

The confidence intervals (CI) of recovery rates with a statistical significance of 5% are also provided in Figure S4. Across all the categories, CI increases with the recovery rate increase, indicating higher uncertainty of recovery rate estimation for exceptionally fast recovery rates. Some evident differences among the land-cover categories are found, particularly in *BL*, which shows larger uncertainties over a range of points that have very fast recovery rates. On the contrary, almost all points of *NL* have low CI, ranging mainly between 0 and 0.03 $month^{-1}$, showing the goodness-of-fit in this case.

Alongside r-square information, an overall good performance of the statistical model applied to the 5 regions of the domain is estimated.

3.6 | Pre- and Post-Fire Assessment

Post-fire vegetation recovery can be modulated by a wide range of factors, namely fire severity, pre-fire vegetation state, and post-fire meteorological conditions (Bright et al. 2019; Viana-Soto et al. 2020; Rifai et al. 2024).

After estimating recovery rates of burned vegetation (b), we calculated the differences between the recovery rate of the

TABLE 1 | Number of pixels in each land-cover category in each region of the domain. The total number of points for each category is also represented.

	BL	NL	Shb	TW
Mediterranean	2730	5040	2580	7321
California	—	4330	3380	11
Australia	10,349	—	2098	775
South Africa	271	—	5345	151
Chile	21	—	32	6
Total	13,371	9370	13,435	8264

second (E_2) and first event (E_1) per-pixel, $b_{DIFF} = b_2 - b_1$. The nonparametric Wilcoxon signed-rank test was applied to compare both distributions and to test if the differences are statistically significantly different from zero. Positive differences ($b_{DIFF} > 0$) indicate faster recovery after E_2 than E_1 (hereafter $b_1 < b_2$), while negative differences ($b_{DIFF} < 0$) indicate faster recovery following E_1 than E_2 (hereafter $b_1 > b_2$). Hence, two groups of pixels were defined based on their recovery rate differences: those with $b_1 < b_2$ and those with $b_1 > b_2$. We analysed these two groups of pixels, $b_1 < b_2$ and $b_1 > b_2$, separately for each land cover-type, selecting pixels with b_{DIFF} falling outside the 25th–75th interquartile range of the distribution to ensure that we sampled pixels where differences were most relevant. Employing more strict constraints, such as selecting differences outside the 10th–90th percentiles would produce similar results but with a smaller and less representative sample size. Therefore, further analysis of fire severity, pre-fire conditions, and post-fire climate variability was performed using the 25th–75th percentiles criteria.

The parameter a of the model fit is used as a proxy of fire severity. To compare across pixels with different greenness levels, we estimated the relative fire severity, a_{REL} as:

$$a_{REL} = \left| \frac{a}{GY_{MEAN}} \right| \quad (5)$$

where GY_{MEAN} is the mean of the annual seasonal cycle of GY at the pixel-level. Due to the negative signal of absolute severity, a, we guarantee, by using the module, that the a_{REL} value ranges from 0 (no severity) towards positive infinity.

First, we analysed the relationship between fire severity and recovery rates by fitting a Kernel Density Estimator (KDE) to the bivariate distribution of a_{REL} and b, grouping pixels in each land-cover class. We separate the two events to evaluate potential changes in this relationship over time and further assess the dependence of recovery rates of burned vegetation on fire severity by performing a quantile regression on the 1st (the least severe fires) and 99th (the most severe fires) quantiles of the relative fire severity distribution.

To analyse the influence of vegetation state before the fire on recovery rates, we estimated at pixel-level the median of $y(t)$ over the 3 months before the fire occurrence, $y(t)_{PRE\text{-}FIRE}$. This value roughly corresponds to the fuel accumulated before the fire season.

We further assess the relationship between recovery rates and post-fire climate variability by analysing the evolution of seasonal standardised anomalies of precipitation and temperature over the 12 months following fire for each pixel and event. The seasonal standardised anomaly was calculated by removing the climatological seasonal mean 2001–2022 and dividing by the seasonal standard deviation 2001–2022. This analysis was conducted by calculating the anomalies at pixel-level, considering each hemisphere's season. The anomalies were further grouped for each condition, i.e., $b_1 < b_2$ and $b_1 > b_2$ across the four land-cover categories.

4 | Results

4.1 | Recovery Rate Assessment

Over the period 2001–2022, several Mediterranean areas experienced recurrent fires (Figure 1, top panel, bar plots): 20%–25% (more than 10%) of the total burned areas in the Mediterranean basin and South Africa (California, Chile, and Australia) burned twice (see also Figure S5). About 10% of the total burned area in this period in the Mediterranean basin, South Africa, and Chile burned three times or more. Frequent fires (more than once) are particularly relevant in the western regions of the Mediterranean basin (Portugal and northern Spain), as well as across southern California, southwestern Australia, and extensive areas of South Africa (Figure S5).

We find important differences in mean recovery rates between the selected regions (Figure 1, bottom panels), with Australia showing the fastest recovery rates (on average 0.10 $month^{-1}$ and characteristic recovery time of about 10 months) and Chile showing the slowest average recovery rates (about 0.04 $month^{-1}$ and characteristic recovery time of 25 months). In the Mediterranean basin, California, and South Africa, the average recovery rate ranges from about 0.05 to 0.065 $month^{-1}$, with a characteristic recovery time of about 15–20 months. Therefore, characteristic recovery times range between 1 year in Australia, 1 year and half in the Mediterranean basin, California, and South Africa, and 2 years in Chile. In the Mediterranean basin, South Africa, and also in California, recovery rates show narrower distributions, indicating more similar recovery rates across pixels within each region, whereas in Australia the flatter distribution indicates larger regional variability in recovery rates (Figure 1, bottom panel).

To evaluate whether there are temporal changes in recovery dynamics, we also compare the distribution of the recovery rate of burned vegetation following each individual fire event in pixels burned twice (Figure 1, bottom panel). On average, recovery tends to be faster following the first event (E_1) compared to the second (E_2) in most regions, except for Chile and the Mediterranean basin, where similar mean recovery rates between the two events are found. Spatially, pixels with larger differences in recovery rates are found particularly in the western sector of the european Mediterranean basin (Portugal and northern Spain), where vegetation recovered faster after E_2 than E_1, and in southern California and western South Africa, where vegetation shows slower recovery after E_2 than E_1 (Figures S6 and S7).

We then compare the dependence of recovery rates on land cover (Figure 3). We find that Needle-leaved forests (*NL*), Shrubland (*Shb*), and Transitional Woodlands (*TW*) tend to show recovery rates with mean values ranging between about 0.05 and 0.065 $month^{-1}$, corresponding to characteristic recovery times of ca. 15–20 months. In turn, Broad-leaved forests (*BL*) tend to show faster recovery times (0.08 $month^{-1}$ and characteristic recovery times of 12 months), as well as larger variability in recovery rates than the other vegetation types, as seen by the broader distributions of recovery rates.

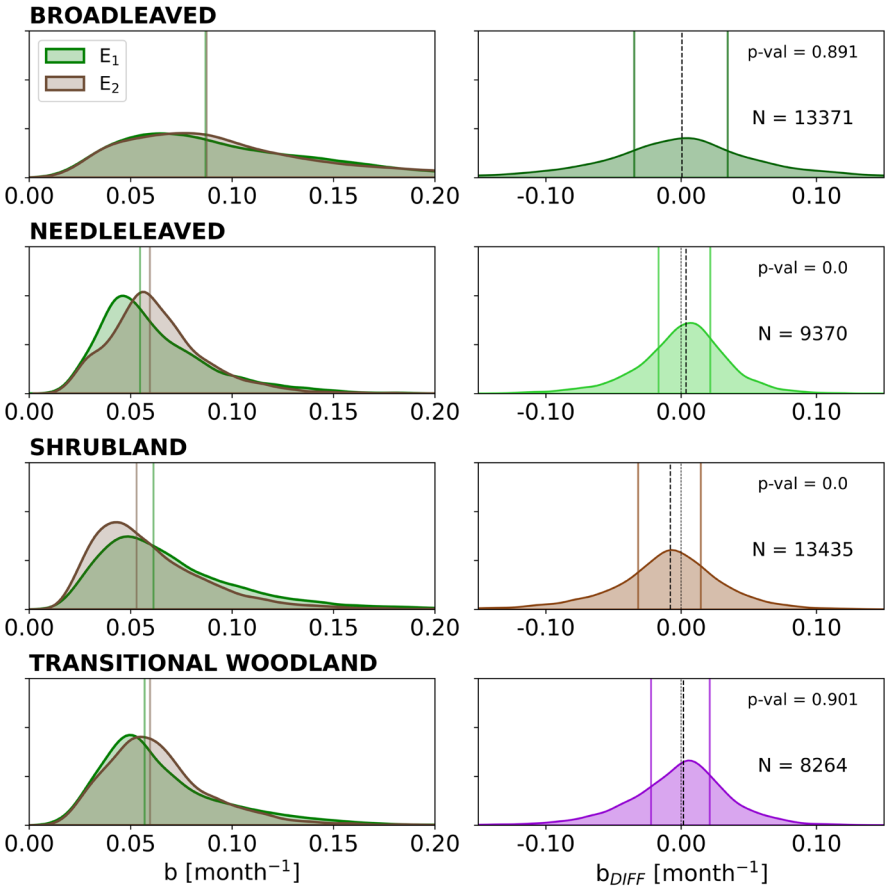

FIGURE 3 | Left panels: Distribution of the recovery rates (b, month^{-1}) of vegetation considering the selected land cover categories for the first fire event, E_1 (green curve), and the second event, E_2 (brown curve). The vertical lines represent the median of each distribution; Right panels: Distribution of differences in recovery rates between the two fire events, b_{DIFF}. The black dashed line describes the median value of b_{DIFF} and the thin grey dashed line is the vertical line of $b_{DIFF} = 0$. The bold lines correspond to the 25th (left side of the distribution) and 75th (right side of the distribution) percentiles of b_{DIFF} in each category. The p-value corresponds to the Wilcoxon signed-rank test applied with a 95% significance.

For *NL* and *Shb*, the distributions of the recovery rates also reveal important differences between fire events. For *NL*, 50% of the pixels show recovery rates faster than 0.059 month^{-1} for E_2, while for E_1 this value is 0.054 month^{-1} (Figure 3, left panels). On average, *NL* generally show faster recovery following E_2 than E_1 by 0.005 month^{-1}, as given by the mean value of the pairwise differences, but also as shown on the displacement of the median values for E_2 compared to E_1, and the left-skewed distribution with positive median of paired differences (Figure 3, right panels). By contrast, in *Shb*, 50% of pixels are showing recovery rates on average faster than 0.053 month^{-1} for E_2 while for E_1, 50% of the distribution recovers at 0.061 month^{-1} or faster (Figure 3, left panel). Hence, *Shb* pixels recover faster after E_1 than E_2 by 0.008 month^{-1}, as given by the mean value of the pairwise differences between and also as shown on the right-skewed distribution and the negative median value of paired differences, which reflects more slower-recovering pixels after E_2 (Figure 3, right panels).

In *BL* and *TW*, the Wilcoxon signed-rank test shows that the median differences between recovery rate distributions are not statistically significant, therefore indicating that E_1 and E_2 distributions are very similar. However, the broad spread of b_{DIFF} distributions can indicate that marked differences in recovery rates between the two events have occurred, but these cancel each other when aggregating spatially. Specifically, *BL* pixels with differences different from zero are found in the Mediterranean basin (positive median, left skewed distribution) and South Africa (negative median, right-skewed distribution) and *TW* pixels with differences different from zero are found in the Mediterranean basin (positive median, left skewed distribution) and Australia (negative median, right-skewed distribution) (Figure S8).

4.2 | Fire Severity

We find a general positive relationship between relative fire severity (a_{REL}) and post-fire recovery rate (b) for each condition and land cover-type (grey points in Figure 4). However, the distribution of the points suggests a marked dependence of this relationship on the relative fire severity. Results of the quantile regression show a strong sensitivity of recovery rates to relative severity in the most severe fires (99th quantile of a_{REL}) for all vegetation types, with slopes ranging between 81 and 147 month^{-1} per relative severity unit. In contrast, for the least severe fires (first quantile of a_{REL}), the recovery rates show low sensitivity to relative severity, with slopes ranging between 6 and 14 month^{-1} (per relative severity unit). Although between the pixel's conditions $b_1 < b_2$ and $b_1 > b_2$ the differences are almost negligible, among the different land

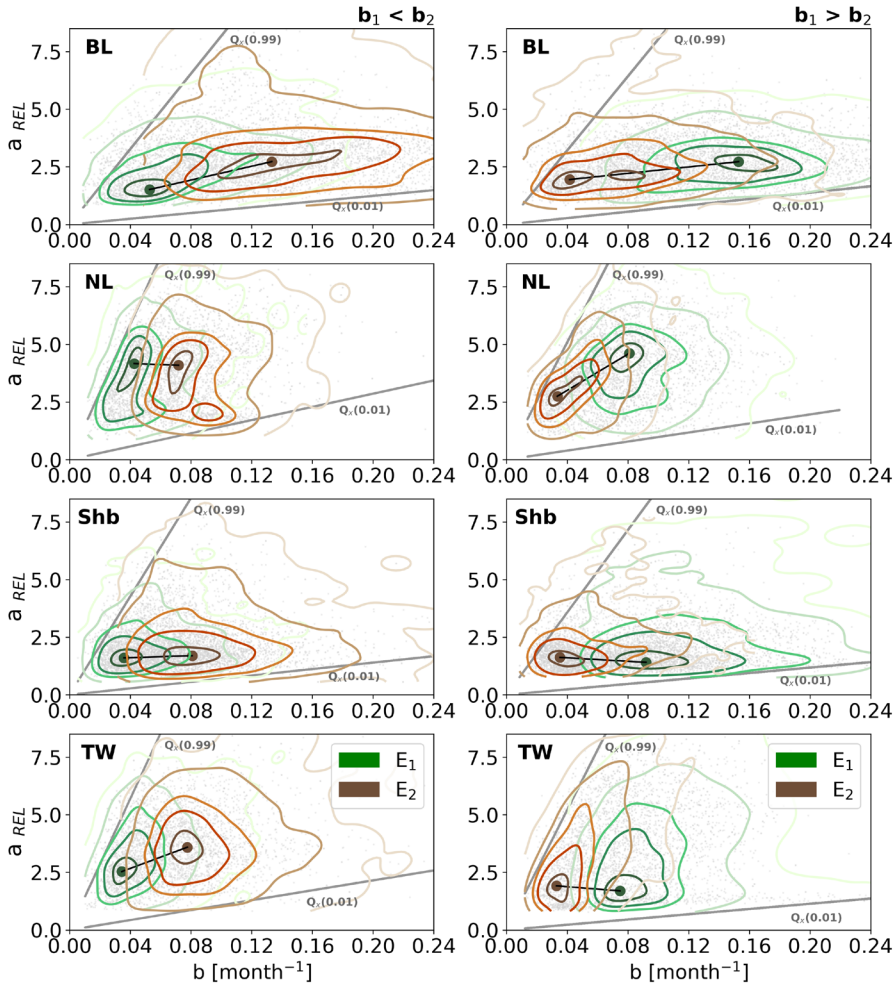

FIGURE 4 | Kernel Density Estimates (KDEs) of the global bivariate distributions of greenness recovery rate, b, and relative severity, a_{REL}, in each land-cover category for E_1 (green) and E_2 (orange) for the group $b_1 < b_2$ (left-side plots) and $b_1 > b_2$ (right-side plots). The distribution of points of the sample of both events is described in grey points. The black line links the centroids of E_1's and E_2's KDEs. The grey lines correspond to the 0.01, Qx(0.01), and the 0.99, Qx(0.99) quantiles of the regression.

cover-types, sharp contrasts within slopes are noticeable. The highest slopes of the quantiles regressions can explain the increasing dependence of the recovery rate of burned vegetation on fire severity. Specifically, *NL* shows the highest slope of the 99th quantile regression (147 and 127 month^{-1} per relative severity unit for $b_1 < b_2$ and $b_1 > b_2$, respectively), followed by *TW* (142 and 130 month^{-1} per relative severity unit for $b_1 < b_2$ and $b_1 > b_2$, respectively). Lower slopes of the 99th quantile regression are found in *Shb* (107 and 89 month^{-1} per relative severity unit for $b_1 < b_2$ and $b_1 > b_2$, respectively) and in *BL*, that shows the lowest values compared to the other land cover-types (82 and 80 month^{-1} per relative severity unit for $b_1 < b_2$ and $b_1 > b_2$, respectively). The same is found for the first quantile regression, with *NL* slopes varying between 10 and 14 month^{-1} per relative severity unit considering both pixel's conditions, and *BL* ranging between 6 and 7 month^{-1} per relative severity unit.

Given the similar configuration of the bivariate relationship between fire severity and recovery rate (a_{REL}, b) for different vegetation types and pixel's conditions, variations in recovery rates per land cover-type and between consecutive events can be partly explained by differences in fire severity. Specifically, in *BL*, *NL* ($b_1 > b_2$) and *TW* ($b_1 < b_2$), the faster recovery rates following E_2 than E_1 are associated with a shift of the bivariate distribution towards higher severity. For the other vegetation types and pixel's conditions, the mean severity is comparable for the two events and, in the case of *Shb* and *TW* ($b_1 < b_2$) relatively small, so that the centroid of the bivariate distribution follows a displacement consistent with the slope of the lowest severity pixels. Exceptions are found in *NL* ($b_1 < b_2$), *Shb* and *TW* ($b_1 > b_2$), where the centroids of the bivariate distribution shifted almost horizontally, indicating that on average, relative severity is similar in both events, but other factors influence vegetation recovery rates.

4.3 | Pre-Fire Vegetation State

We then analyse how pre-fire vegetation condition, $y(t)_{PRE\text{-}FIRE}$, varies across different values of recovery rates and fire severity for each land-cover category (Figure 5) and for the conditions $b_1 < b_2$ (left panel) and $b_1 > b_2$ (right panel).

Compared to other vegetation types, *BL* exhibits overall lower $y(t)_{PRE\text{-}FIRE}$, for both conditions across different levels of relative fire severity. In turn, *Shb* consistently shows a state closer to the

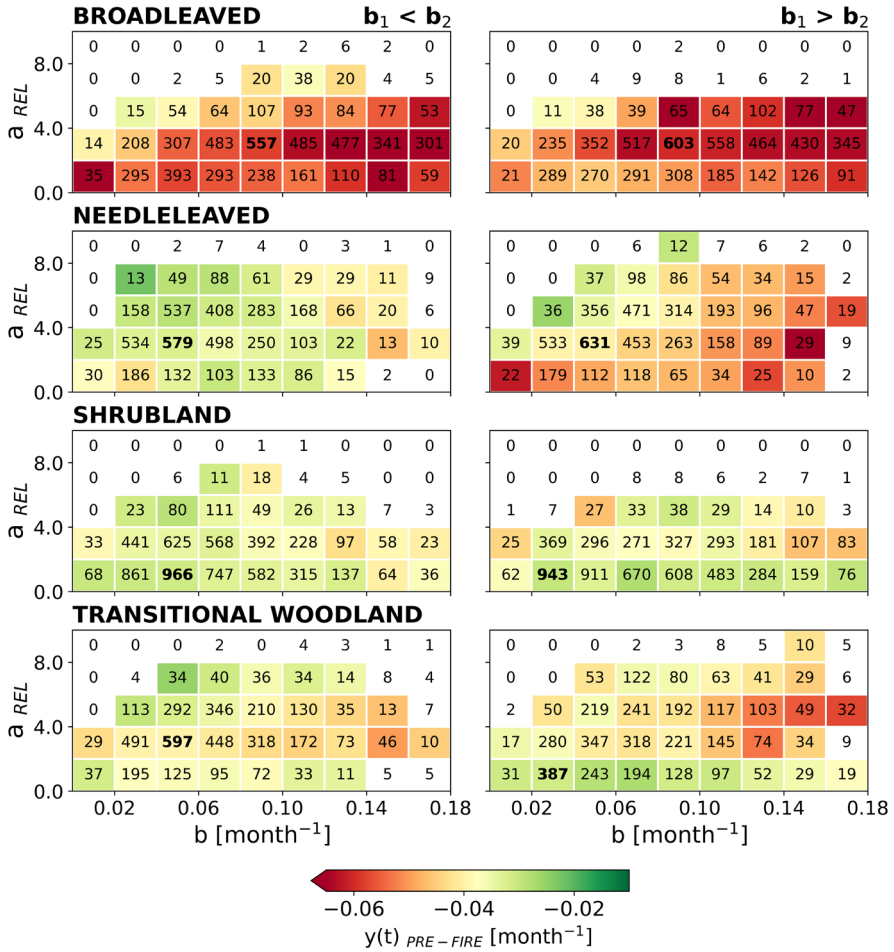

FIGURE 5 | Diagram of the bivariate distribution of greenness recovery rate, b, and relative severity, a_{REL}, binned for different levels of $y(t)_{PRE\text{-}FIRE}$, considering each land-cover category when $b_1 < b_2$ in (left panels) and $b_1 > b_2$ (right panels). The number of points within each bin is described and the number represented in bold corresponds to the bin which presents the highest number of points.

ideal in both conditions and for most levels of a_{REL} and b, suggesting a weaker influence of pre-fire conditions of vegetation on relative fire severity and thereby on recovery rate.

Predominantly larger departures from the ideal seasonal cycle are found for intermediate levels of relative severity in most vegetation types, which can be associated with higher availability of fine and dry fuels from leaf shedding under stress resulting in more intense fires. For similar levels of relative fire severity, more strongly negative values of $y(t)_{PRE\text{-}FIRE}$ tend to be associated with faster recovery rates for *BL* in both cases, for *NL* ($b_1 < b_2$) and for *Shb* ($b_1 > b_2$) and *TW* ($b_1 > b_2$), which can explain why the bivariate distribution of (a_{REL}, b) in these cases shifts horizontally. On the other hand, closer to ideal seasonal cycle values of $y(t)_{PRE\text{-}FIRE}$ tend to be associated with more severe fires and slower recovery rates. This is observed for *NL* and *TW* in both conditions and *BL* ($b_1 < b_2$).

4.4 | Post-Fire Climate Variability

Finally, climate variability during the recovery period might contribute to modulate recovery rates. We find that faster recovery of burned vegetation can be enhanced due to the availability of water or favourable temperatures, or even the conjunction of both conditions. By contrast, slow-recovery pixels tend to be associated with negative anomalies of precipitation and high temperatures, with variations between vegetation types (Figure 6). For *Shb*, slow-recovery rates are associated with precipitation deficits in the second quartile following the fire season (Q2, typically corresponding to local spring), in conjunction with positive temperature anomalies in the following Q3 (local summer) for all events analysed. The same is found for *BL* ($b_1 < b_2$). For the *BL*, *NL*, *Shb*, and *TW* pixels showing slower recovery rates following E_2 than E_1, the delay is predominantly associated with low rainfall with high temperatures in the autumn at the end of the subsequent growing season (Q4). By contrast, higher precipitation in Q4 results in faster recovery rates for *NL* and *Shb* following E_2, compared to E_1.

The persistence of positive precipitation anomalies immediately following the fire (Q1) can, however, promote a slower recovery rate, as seen in *NL* ($b_1 > b_2$).

5 | Discussion

Here we provide a first assessment of vegetation recovery dynamics across the Mediterranean biome following repeated fires. We find predominantly faster recovery rates for broad-leaved

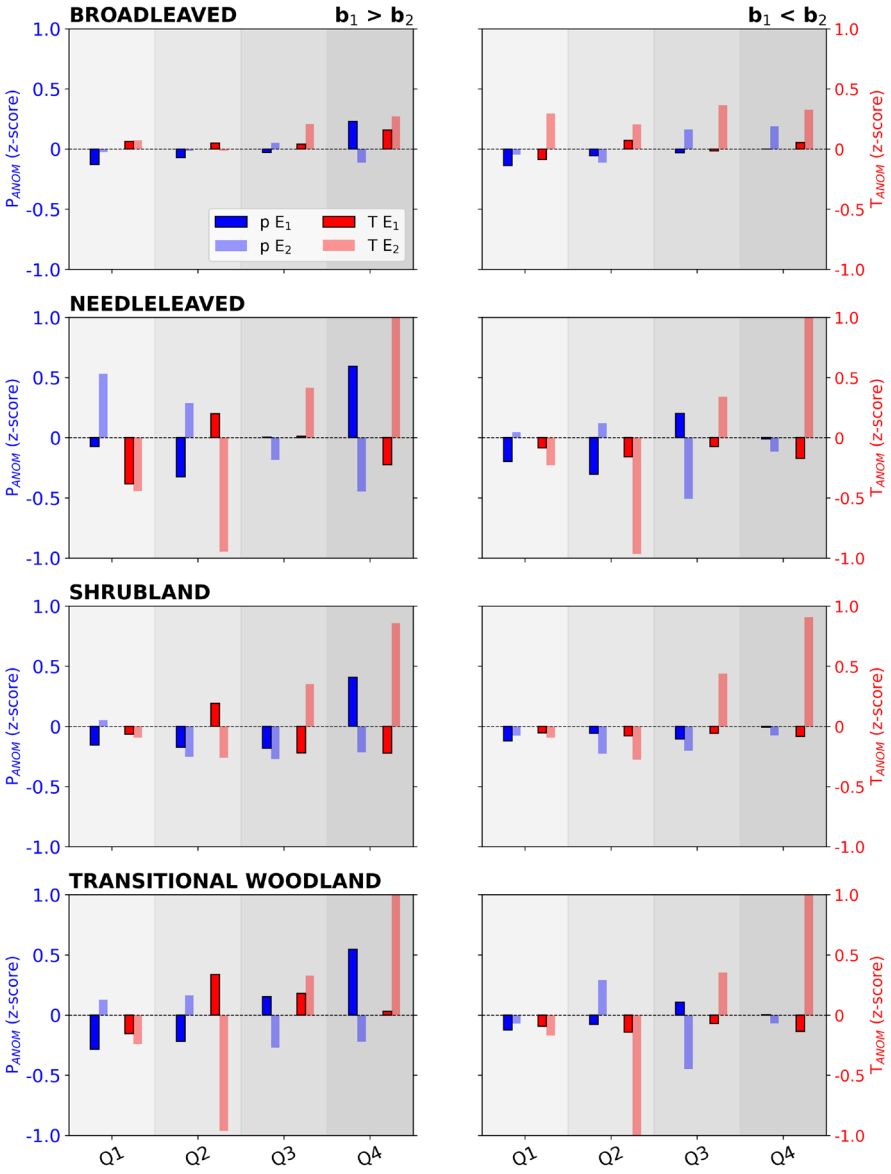

FIGURE 6 | Post-fire standardised anomalies (*z*-score) of precipitation (blue bars and blue axis) and temperature (red bars and red axis) after E_1 and E_2. The anomalies are determined for both conditions, $b_1 > b_2$ (left panels) and $b_1 < b_2$ (right panels) in each land-cover category, and for the following four quarters of months (Q1–Q4) after the fire occurrence. The shaded areas differentiate each quarter. The bars in bold are representative of the fire event whose pixels had a higher recovery rate.

forests, compared to needle-leaved forests, transitional woodlands and shrublands across the study region (Figure 1). Large variability in differences in recovery rates between the first and second fire events is found, explained by regional differences in vegetation type, but also post-fire climate variability and fire severity. In general, mean recovery rate tends to be faster after E_1 than E_2, although regional differences are detected. Specifically, needle-leaved forests of the western Mediterranean basin and southern California show predominantly faster recovery after E_2 than E_1. Burned vegetation from Australia and the Mediterranean basin, particularly broad-leaved forests, is associated with higher recovery rates and no significant differences between fire events were detected. Broad-leaved forests in the Mediterranean regions tend to be well adapted to fire, for example through resprouting ability or bark protection mechanisms, which allow for quick recovery of greenness following the fire (Pausas and Keeley 2009; Losso et al. 2022). Vegetation from South Africa, northern California and some areas of the eastern Mediterranean basin tend to be associated with slower recovery rates following E_2 than E_1, particularly due to the higher distribution of shrublands. As broad-leaved forests, Mediterranean shrublands are also well adapted to fire, especially the ecosystems highly covered with obligate resprouters species. However, repeated fires can deplete resprouters species in ecosystems, which can be gradually replaced by more flammable shrubland populations such as obligate seeders. Together with post-fire hotter and drier conditions, the obligate seeders communities can decrease the recovery rate of vegetation after recurrent fires and reduce the resilience of the ecosystem (Pausas and Keeley 2009; Keeley et al. 2012; Calvo et al. 2011; Salesa et al. 2022).

We find an emerging relationship between post-fire recovery rates and relative fire severity across different vegetation types, with increasing dependence of recovery rates on fire severity

with increasing fire severity (Figure 3). Mediterranean ecosystems tend to be adapted to fire, and some species have reproduction mechanisms that are activated by fire, such as the release and dispersal of seeds in soils from seed banks (Bright et al. 2019; Harrison et al. 2021; Landesmann et al. 2021; Falk et al. 2022). For similar levels of fire severity, and especially for extreme severity levels, most pixels tend to show slower recovery rates. Extremely severe fires, e.g., stand-replacing fires, can eliminate or impair vegetation mechanisms to recover (Falk et al. 2022), and lead to low rates of burned ecosystems recovery. In this analysis, we have focused on pixels where repeated fires did not result in changes in vegetation type, which likely explains the characteristic shape of the bivariate distribution between fire severity and recovery rates.

We also find a modulation effect on post-fire recovery rates by the pre-fire vegetation conditions, through two pathways: (i) higher levels of pre-fire greenness tend to be associated with highly severe fires, resulting in slower recovery rates; (ii) low levels of pre-fire greenness tend to be associated with faster recovery rates. One plausible explanation for (i) is that high pre-fire greenness, likely indicating healthy and productive vegetation, may be associated with dense live vegetation and significant fuel accumulation, available for combustion (Roberts et al. 2003; Parks et al. 2014). Thus, the fire propagation and severity can be exacerbated under summer hot and dry conditions, as pinpointed in several studies carried out on burned patches mainly composed of pines and eucalyptus in Mediterranean ecosystems (Gouveia et al. 2012, 2016; David et al. 2016; García-Llamas et al. 2019; Ermitão et al. 2022), consequently leading to longer recovery periods. By contrast, larger departures from the ideal seasonal cycle prior to the fire event (ii) reflect loss of vegetation vitality or density prior to the fire event. In that case, faster recovery might be explained by reduced competition for resources between surviving or rapidly reestablishing vegetation. This might explain why the effect of pre-fire condition is most pronounced in broad-leaved forests, where competition for light following fire is likely to play an important role (Pausas and Keeley 2009).

We further showed that post-fire climate conditions can modulate recovery rates, explaining differences in recovery between the first and second fires. Post-fire water availability played a particularly important role, not only during the growing season following the fire event but also afterwards. A faster recovery was found for pixels with sufficient water availability and normal to slightly higher than climatological mean temperatures. These results are consistent with the fact that vegetation dynamics in these semi-arid regions tends to be water-limited (Gouveia, Trigo, and DaCamara 2009; Gouveia et al. 2017; Vicente-Serrano 2006; Barkaoui et al. 2017; Ermitão et al. 2021; Rodrigues et al. 2024). For example, Meng et al. (2015) observed that the wet season after fire and temperatures in winter might be favourable in mixed conifer forests in California whereas Blanco-Rodríguez et al. (2023) highlighted that post-fire vegetation recovery in the first year is strongly conditioned by drought duration across western Mediterranean basin. We also show that rainfall deficits combined with high temperatures in the 9–12 months following the fire hampered recovery in all vegetation types. While increased water availability tends to favour recovery, we also found that persistent positive precipitation anomalies during the 3 months immediately after the fire were associated with slower recovery rates, especially for needle-leaved forests. A possible explanation could be that excessive rainfall in the first months after the fire can increase top-soil erosion and drag or destroy the seed banks released from burned trees, hampering the recovery capacity, as seen in Auld et al. (2020) after the 2019/2020 fire season in Australia. Post-fire erosion events have been previously reported in several other regions, especially those with high slopes, such as central Portugal (Melo, van Asch, and Zêzere 2018), southern Italy (Esposito et al. 2023), or southern California (Cheung and Giardino 2023).

Our study shows that vegetation recovery is a complex process, depending on a large set of variables that are themselves interrelated, such as fire severity, pre-fire vegetation condition and post-fire climate variability. To better understand these relationships, long time-series and finely resolved information in space is needed. We analysed the areas that burned twice, as the fire return periods for the Mediterranean regions are on average 20 years (Archibald et al. 2013; Harrison et al. 2021). Hence, this constrains our approach because our time-series are still quite short (about 20 years) to assess recovery in other regions of the world where fire return intervals and recovery are much longer (50–100 years), such as the boreal regions (Harrison et al. 2021). Furthermore, our approach for recovery estimation is based on the vegetation greenness index EVI, which effectively captures the impact of the fire on vegetation, as it is highly sensitive to fire events and reflects the initial stages of vegetation recovery through leaf resprouting (Bousquet et al. 2022). However, we note that EVI cannot fully capture the restoration of aboveground biomass (AGB) and carbon (AGC), particularly since AGB, which is heavily impacted by fire, often begins to recover only several months after the event, as seen in Bousquet et al. (2022) among different biomes and in Fan et al. (2023) over boreal regions. This limitation could be overcome by using other satellite-based datasets that better capture aboveground biomass dynamics such as Radar, or LiDAR, but such datasets are only available at very coarse spatial resolution and have shorter temporal coverage (Pérez-Cabello, Montorio, and Alves 2021; Qin et al. 2022; Fan et al. 2023), that is not compatible with the aim of long term recovery and resilience assessment.

We note that other fire-related variables, such as topography, biomass accumulation, land management, or human intervention, are also likely to affect the recovery of burned ecosystems, and can be considered in future studies. On the other hand, despite the quality analysis, we are aware that land-cover products may have classification errors that can not fully capture changes in vegetation, constituting a source of uncertainty, although we use an approach that aims to ensure that the land cover-type is the same before both fire events, partly mitigating the effect of land-cover shifts in the specific pixel. Moreover, it should also be stressed that we are interested in evaluating the recovery rate of greenness considering different vegetation types frequently disturbed by wildfires within Mediterranean ecosystems, and we do not work towards the estimation of specific recovery times and their phenology. Notwithstanding, our approach shows the value of estimating recovery dynamics based on time-series rather than space-for-time substitution, analysing how pre-fire conditions and fire severity modulate recovery dynamics comparing recurrent events. More frequent or intense hot and dry

conditions under climate change can hamper the recovery process, especially in regions with typically high fuel loads, which can in turn result in severe and prolonged damage to ecosystems. While Mediterranean ecosystems are adapted to fire, changes in fire recurrence and increasing water deficits can further limit vegetation's ability to recover, by reducing, for example, post-fire seedling densities (Rodman et al. 2020).

6 | Conclusions

This study proposes an assessment of how the Mediterranean biome throughout the world has been recovering from recurrent fires, relying on a mono-parametric statistical model applied to a time-series of spectral index EVI that evaluates the rate of recovery of vegetation greenness following fires. Although well adapted to fire, the Mediterranean ecosystems under climate change are vulnerable to increasing fire severity and unfavourable post-fire conditions, making it essential to understand the multiple factors that influence vegetation recovery dynamics.

Here, we find that the mean recovery rate of burned vegetation tends to be faster after the first event than the second event, although we detect large variability between recovery rates, which are roughly attributed to regional contrasts in different vegetation types, and also fire severity and post-fire climate conditions. In particular, needle-leaved forests tend to recover faster after the second event, whereas shrublands contrast by showing faster recovery following the first event. Broad-leaved forests and transitional woodlands show no statistically significant differences in recovery rate distributions, although their broad spread suggests marked regional differences, particularly in areas such as in the Mediterranean basin.

Our results show that fire severity modulates recovery dynamics, as recovery rates are enhanced with increasing severity. However, extremely severe fires are followed by very slow recovery, and these events are strongly associated with high values of pre-fire greenness of vegetation, particularly in forest ecosystems. We further find that post-fire climate variability modulates the rates of vegetation recovery. Precipitation availability, associated with normal to above-mean temperatures in the growing season, seems to favour vegetation greenness recovery. This reflects the importance of water availability in these ecosystems and shows how precipitation and temperature changes in the future might affect the regeneration of recurrently burned ecosystems.

The overall consistency of the results shows the good performance of the proposed methodology, which enhances the value of using a time-series approach combined with a mono-parametric model to determine the recovery rates of burned vegetation, rather than space-for-time substitution methods, providing a reliable tool for understanding post-fire recovery dynamics.

Author Contributions

Tiago Ermitão: conceptualization, data curation, formal analysis, investigation, methodology, writing – original draft, writing – review and editing. **Célia M. Gouveia:** conceptualization, formal analysis, investigation, methodology, resources, writing – review and editing. **Ana Bastos:** conceptualization, formal analysis, investigation, writing – review and editing. **Ana C. Russo:** conceptualization, funding acquisition, investigation, project administration, resources, writing – review and editing.

Acknowledgments

T.E. was supported by the doctoral Grant PRT/BD/154296/2022 financed by the Portuguese Fundação para a Ciência e a Tecnologia (FCT) under the MIT Portugal Program. T.E. would also like to acknowledge the support of the Max-Planck Institute for Biogeochemistry and University of Leipzig in this work. This study was performed under the framework of the DHEFEUS project, funded by FCT (https://doi.org/10.54499/2022.09185.PTDC). A.R. is supported by the FCT through national funds from the MCTES within the Faculty of Sciences of the University of Lisbon, through https://doi.org/10.54499/2022.01167.CEECIND/CP1722/CT0006. A.B. acknowledges funding by the European Union (ERC StG, ForExD, grant agreement No. 101039567).

Conflicts of Interest

The authors declare no conflicts of interest.

Data Availability Statement

The data and code used to generate the main results of this study are available in Zenodo at https://doi.org/10.5281/zenodo.14477670. EVI and burn area data were obtained from the NASA EOSDIS Land Processes Distributed Active Archive Center at https://doi.org/10.5067/MODIS/MOD13A1.061 and https://doi.org/10.5067/MODIS/MCD64A1.061, respectively. Land cover data were obtained from the ESA Climate Change Initiative and in particular its Land Cover project at https://maps.elie.ucl.ac.be/CCI/viewer/download.php (version 2.0.8). Precipitation and air temperature were obtained from Copernicus at https://doi.org/10.24381/cds.e2161bac.

References

Anderegg, W. R., J. M. Kane, and L. D. Anderegg. 2013. "Consequences of Widespread Tree Mortality Triggered by Drought and Temperature Stress." *Nature Climate Change* 3, no. 1: 30–36.

Archibald, S., C. E. Lehmann, J. L. Gómez-Dans, and R. A. Bradstock. 2013. "Defining Pyromes and Global Syndromes of Fire Regimes." *Proceedings of the National Academy of Sciences of the United States of America* 110, no. 16: 6442–6447.

Auld, T. D., B. Mackenzie, T. Le Breton, et al. 2020. *A Preliminary Assessment of the Impact of the 2019/2020 Fires on NSW Plants of National Significance*. Parramatta: NSW Government Department of Planning Industry and Environment.

Baeza, M. J., A. Valdecantos, J. A. Alloza, and V. R. Vallejo. 2007. "Human Disturbance and Environmental Factors as Drivers of Long-Term Post-Fire Regeneration Patterns in Mediterranean Forests." *Journal of Vegetation Science* 18, no. 2: 243–252.

Barkaoui, K., M. L. Navas, C. Roumet, P. Cruz, and F. Volaire. 2017. "Does Water Shortage Generate Water Stress? An Ecohydrological Approach Across Mediterranean Plant Communities." *Functional Ecology* 31, no. 6: 1325–1335.

Bastos, A., P. Ciais, P. Friedlingstein, et al. 2020. "Direct and Seasonal Legacy Effects of the 2018 Heat Wave and Drought on European Ecosystem Productivity." *Science Advances* 6, no. 24: eaba2724.

Bastos, A., C. M. Gouveia, C. C. DaCamara, and R. M. Trigo. 2011. "Modelling Post-Fire Vegetation Recovery in Portugal." *Biogeosciences* 8, no. 12: 3593–3607.

Bastos, A., R. Orth, M. Reichstein, et al. 2021. "Vulnerability of European Ecosystems to Two Compound Dry and Hot Summers in 2018 and 2019." *Earth System Dynamics* 12, no. 4: 1015–1035.

Bastos, A., S. Sippel, D. Frank, et al. 2023. "A Joint Framework for Studying Compound Ecoclimatic Events." *Nature Reviews Earth and Environment* 4, no. 5: 333–350.

Blanco-Rodríguez, M. Á., A. Ameztegui, P. Gelabert, M. Rodrigues, and L. Coll. 2023. "Short-Term Recovery of Post-Fire Vegetation Is Primarily Limited by Drought in Mediterranean Forest Ecosystems." *Fire Ecology* 19, no. 1: 68.

Bousquet, E., A. Mialon, N. Rodriguez-Fernandez, S. Mermoz, and Y. Kerr. 2022. "Monitoring Post-Fire Recovery of Various Vegetation Biomes Using Multi-Wavelength Satellite Remote Sensing." *Biogeosciences* 19, no. 13: 3317–3336.

Bowman, D. M., A. Moreira-Muñoz, C. A. Kolden, et al. 2019. "Human–Environmental Drivers and Impacts of the Globally Extreme 2017 Chilean Fires." *Ambio* 48: 350–362.

Brennan, J., J. L. Gómez-Dans, M. Disney, and P. Lewis. 2019. "Theoretical Uncertainties for Global Satellite-Derived Burned Area Estimates." *Biogeosciences* 16, no. 16: 3147–3164.

Bright, B. C., A. T. Hudak, R. E. Kennedy, J. D. Braaten, and A. Henareh Khalyani. 2019. "Examining Post-Fire Vegetation Recovery With Landsat Time Series Analysis in Three Western North American Forest Types." *Fire Ecology* 15, no. 1: 1–14.

Brito-Morales, I., J. G. Molinos, D. S. Schoeman, et al. 2018. "Climate Velocity Can Inform Conservation in a Warming World." *Trends in Ecology & Evolution* 33, no. 6: 441–457.

Brown, T., S. Leach, B. Wachter, and B. Gardunio. 2020. "The Extreme 2018 Northern California Fire Season." *Bulletin of the American Meteorological Society* 101: S1–S4.

Byrne, B., J. Liu, K. W. Bowman, et al. 2024. "Carbon Emissions From the 2023 Canadian Wildfires." *Nature* 633: 835–839.

Calvo, L., J. Baeza, E. Marcos, V. Santana, and V. P. Papanastasis. 2011. "Post-Fire Management of Shrublands." In *Post-Fire Management and Restoration of Southern European Forests*, edited by F. Moreira, M. A. P. Corona, and J. D. L. Heras, 293–319. Dordrecht: Springer Netherlands.

Cheung, D. J., and J. R. Giardino. 2023. "Debris Flow Occurrence Under Changing Climate and Wildfire Regimes: A Southern California Perspective." *Geomorphology* 422: 108538.

Clarke, P. J., M. J. Lawes, J. J. Midgley, et al. 2013. "Resprouting as a Key Functional Trait: How Buds, Protection and Resources Drive Persistence After Fire." *New Phytologist* 197, no. 1: 19–35.

Cleveland, R. B., W. S. Cleveland, J. E. McRae, and I. Terpenning. 1990. "STL: A Seasonal-Trend Decomposition." *Journal of Official Statistics* 6, no. 1: 3–73.

Cordero, R. R., S. Feron, A. Damiani, et al. 2024. "Extreme Fire Weather in Chile Driven by Climate Change and El Niño–Southern Oscillation (ENSO)." *Scientific Reports* 14: 1974.

David, T. S., C. A. Pinto, N. Nadezhdina, and J. S. David. 2016. "Water and Forests in the Mediterranean Hot Climate Zone: A Review Based on a Hydraulic Interpretation of Tree Functioning." *Forestry Systems* 25, no. 2: 12.

Davis, M. B., R. G. Shaw, and J. R. Etterson. 2005. "Evolutionary Responses to Changing Climate." *Ecology* 86, no. 7: 1704–1714.

De Luca, G., J. M. Silva, and G. Modica. 2022. "Short-Term Temporal and Spatial Analysis for Post-Fire Vegetation Regrowth Characterization and Mapping in a Mediterranean Ecosystem Using Optical and SAR Image Time-Series." *Geocarto International* 37, no. 27: 15428–15462.

Di Gregorio, A. 2005. *Land Cover Classification System: Classification Concepts and User Manual: LCCS*. Rome, Italy: Food & Agriculture Organization.

Díaz-Delgado, R., F. Lloret, X. Pons, and J. Terradas. 2002. "Satellite Evidence of Decreasing Resilience in Mediterranean Plant Communities After Recurrent Wildfires." *Ecology* 83, no. 8: 2293–2303.

Díaz-Delgado, R., and X. Pons. 2001. "Spatial Patterns of Forest Fires in Catalonia (NE of Spain) Along the Period 1975–1995. Analysis of Vegetation Recovery After Fire." *Forest Ecology and Management* 147: 67–74.

Didan, K., A. B. Munoz, R. Solano, and A. Huete. 2015. *MODIS Vegetation Index User's Guide (MOD13 Series)*. Tucson, AZ: University of Arizona: Vegetation Index and Phenology Lab.

Dinerstein, E., D. Olson, A. Joshi, et al. 2017. "An Ecoregion-Based Approach to Protecting Half the Terrestrial Realm." *BioScience* 67, no. 6: 534–545.

Donato, D. C., J. B. Fontaine, J. L. Campbell, W. D. Robinson, J. B. Kauffman, and B. E. Law. 2009. "Conifer Regeneration in Stand-Replacement Portions of a Large Mixed-Severity Wildfire in the Klamath-Siskiyou Mountains." *Canadian Journal of Forest Research* 39: 823–838.

Dosiou, A., I. Athinelis, E. Katris, et al. 2024. "Employing Copernicus Land Service and Sentinel-2 Satellite Mission Data to Assess the Spatial Dynamics and Distribution of the Extreme Forest Fires of 2023 in Greece." *Fire* 7, no. 1: 20.

Epting, J., and J. Verbyla. 2005. "Landscape-Level Interactions of Prefire Vegetation, Burn Severity, and Postfire Vegetation Over a 16-Year Period in Interior Alaska." *Canadian Journal of Forest Research* 35: 1367–1377.

Ermitão, T., C. M. Gouveia, A. Bastos, and A. C. Russo. 2021. "Vegetation Productivity Losses Linked to Mediterranean Hot and Dry Events." *Remote Sensing* 13: 4010.

Ermitão, T., C. M. Gouveia, A. Bastos, and A. C. Russo. 2022. "Interactions Between Hot and Dry Fuel Conditions and Vegetation Dynamics in the 2017 Fire Season in Portugal." *Environmental Research Letters* 17, no. 9: 095009.

Ermitão, T., P. Páscoa, I. Trigo, C. Alonso, and C. Gouveia. 2023. "Mapping the Most Susceptible Regions to Fire in Portugal." *Fire* 6, no. 7: 254.

Esposito, G., S. L. Gariano, R. Masi, S. Alfano, and G. Giannatiempo. 2023. "Rainfall Conditions Leading to Runoff-Initiated Post-Fire Debris Flows in Campania, Southern Italy." *Geomorphology* 423: 108557.

Etchells, H., A. J. O'Donnell, W. L. McCaw, and P. F. Grierson. 2020. "Fire Severity Impacts on Tree Mortality and Post-Fire Recruitment in Tall Eucalypt Forests of Southwest Australia." *Forest Ecology and Management* 459: 117850.

Evelpidou, N., M. Tzouxanioti, T. Gavalas, et al. 2021. "Assessment of Fire Effects on Surface Runoff Erosion Susceptibility: The Case of the Summer 2021 Forest Fires in Greece." *Land* 11, no. 1: 21.

Falk, D. A., P. J. van Mantgem, J. E. Keeley, et al. 2022. "Mechanisms of Forest Resilience." *Forest Ecology and Management* 512: 120129.

Falk, D. A., A. C. Watts, and A. E. Thode. 2019. "Scaling Ecological Resilience." *Frontiers in Ecology and Evolution* 7: 275.

Fan, L., J. P. Wigneron, P. Ciais, et al. 2023. "Siberian Carbon Sink Reduced by Forest Disturbances." *Nature Geoscience* 16, no. 1: 56–62.

Filkov, A. I., T. Ngo, S. Matthews, S. Telfer, and T. D. Penman. 2020. "Impact of Australia's Catastrophic 2019/20 Bushfire Season on Communities and Environment. Retrospective Analysis and Current Trends." *Journal of Safety Science and Resilience* 1, no. 1: 44–56.

García-Llamas, P., S. Suárez-Seoane, A. Taboada, et al. 2019. "Environmental Drivers of Fire Severity in Extreme Fire Events That Affect Mediterranean Pine Forest Ecosystems." *Forest Ecology and Management* 433: 24–32.

Giglio, L., L. Boschetti, D. P. Roy, M. L. Humber, and C. O. Justice. 2018. "The Collection 6 MODIS Burned Area Mapping Algorithm and Product." *Remote Sensing of Environment* 217: 72–85.

Gouveia, C., C. C. DaCamara, and R. M. Trigo. 2010. "Post-Fire Vegetation Recovery in Portugal Based on Spot/Vegetation Data." *Natural Hazards and Earth System Sciences* 10, no. 4: 673–684.

Gouveia, C., P. Páscoa, and C. DaCamara. 2018. "Post-Fire Vegetation Recovery in Iberia Based on Remote-Sensing Information." In *Forest Fire*, edited by J. Szmyt. London: Intechopen.

Gouveia, C., R. Trigo, and C. DaCamara. 2009. "Drought and Vegetation Stress Monitoring in Portugal Using Satellite Data." *Natural Hazards and Earth System Sciences* 2009, no. 9: 185–195.

Gouveia, C. M., A. Bastos, R. M. Trigo, and C. C. DaCamara. 2012. "Drought Impacts on Vegetation in the Pre-and Post-Fire Events Over Iberian Peninsula." *Natural Hazards and Earth System Sciences* 12, no. 10: 3123–3137.

Gouveia, C. M., I. Bistinas, M. L. Liberato, A. Bastos, N. Koutsias, and R. Trigo. 2016. "The Outstanding Synergy Between Drought, Heatwaves and Fuel on the 2007 Southern Greece Exceptional Fire Season." *Agricultural and Forest Meteorology* 218: 135–145.

Gouveia, C. M., R. M. Trigo, S. Beguería, and S. M. Vicente-Serrano. 2017. "Drought Impacts on Vegetation Activity in the Mediterranean Region: An Assessment Using Remote Sensing Data and Multi-Scale Drought Indicators." *Global and Planetary Change* 151: 15–27.

Harrison, S. P., I. C. Prentice, K. J. Bloomfield, et al. 2021. "Understanding and Modelling Wildfire Regimes: An Ecological Perspective." *Environmental Research Letters* 16, no. 12: 125008.

Higuera, P. E., and J. T. Abatzoglou. 2021. "Record-Setting Climate Enabled the Extraordinary 2020 Fire Season in the Western United States." *Global Change Biology* 27: 1–2.

Hislop, S., S. Jones, M. Soto-Berelov, A. Skidmore, A. Haywood, and T. H. Nguyen. 2018. "Using Landsat Spectral Indices in Time-Series to Assess Wildfire Disturbance and Recovery." *Remote Sensing* 10, no. 3: 460.

Huete, A., K. Didan, T. Miura, E. P. Rodriguez, X. Gao, and L. G. Ferreira. 2002. "Overview of the Radiometric and Biophysical Performance of the MODIS Vegetation Indices." *Remote Sensing of Environment* 83, no. 1–2: 195–213.

Jones, M. W., J. T. Abatzoglou, S. Veraverbeke, et al. 2022. "Global and Regional Trends and Drivers of Fire Under Climate Change." *Reviews of Geophysics* 60, no. 3: e2020RG000726.

Jones, M. W., S. Veraverbeke, N. Andela, et al. 2024. "Global Rise in Forest Fire Emissions Linked to Climate Change in the Extratropics." *Science* 386, no. 6719: eadl5889.

Keeley, J. E., W. J. Bond, R. A. Bradstock, J. G. Pausas, and P. W. L. Rundel. 2012. *Fire in Mediterranean Ecosystems. Ecology, Evolution and Management*. Cambridge: Cambridge University Press.

Kirches, G., C. Brockmann, M. Boettcher, et al. 2014. *Land Cover CCI-Product User Guide-Version 2*. Belgium: ESA Public Document CCI-LC-PUG, UCL-Geomatics.

Köppen, W. P. 1936. *Das Geographische System der Klimate: Mit 14 Textfiguren*. Berlin: Borntraeger.

Landesmann, J. B., F. Tiribelli, J. Paritsis, T. T. Veblen, and T. Kitzberger. 2021. "Increased Fire Severity Triggers Positive Feedbacks of Greater Vegetation Flammability and Favors Plant Community-Type Conversions." *Journal of Vegetation Science* 32, no. 1: e12936.

Lawes, M. J., and P. J. Clarke. 2011. "Ecology of Plant Resprouting: Populations to Community Responses in Fire-Prone Ecosystems." *Plant Ecology* 212: 1937–1943.

Liu, X., L. Yu, Y. Si, et al. 2018. "Identifying Patterns and Hotspots of Global Land Cover Transitions Using the ESA CCI Land Cover Dataset." *Remote Sensing Letters* 9, no. 10: 972–981.

Liu, Z. 2016. "Effects of Climate and Fire on Short-Term Vegetation Recovery in the Boreal Larch Forests of Northeastern China." *Scientific Reports* 6: 37572.

Liu, Z., J. M. Eden, B. Dieppois, W. S. Conradie, and M. Blackett. 2023. "The April 2021 Cape Town Wildfire: Has Anthropogenic Climate Change Altered the Likelihood of Extreme Fire Weather?" *Bulletin of the American Meteorological Society* 104, no. 1: E298–E304.

Los, S. O. 1998. "Linkages Between Global Vegetation and Climate: An Analysis Based on NOAA-Advanced Very High Resolution Radiometer Data." PhD thesis, Vrije Universiteit, Amsterdam, 179 pp.

Losso, A., A. Challis, A. Gauthey, et al. 2022. "Canopy Dieback and Recovery in Australian Native Forests Following Extreme Drought." *Scientific Reports* 12, no. 1: 21608.

McCarthy, G. J., M. P. Plucinski, and J. S. Gould. 2012. "Analysis of the Resourcing and Containment of Multiple Remote Fires: The Great Divide Complex of Fires, Victoria, December 2006." *Australian Forestry* 75, no. 1: 54–63.

McWethy, D. B., A. Pauchard, R. A. García, et al. 2018. "Landscape Drivers of Recent Fire Activity (2001–2017) in South-Central Chile." *PLoS One* 13, no. 8: e0201195.

Melo, R., T. van Asch, and J. L. Zêzere. 2018. "Debris Flow Run-Out Simulation and Analysis Using a Dynamic Model." *Natural Hazards and Earth System Sciences* 18, no. 2: 555–570.

Meng, R., P. E. Dennison, C. Huang, M. A. Moritz, and C. D'Antonio. 2015. "Effects of Fire Severity and Post-Fire Climate on Short-Term Vegetation Recovery of Mixed-Conifer and Red Fir Forests in the Sierra Nevada Mountains of California." *Remote Sensing of Environment* 171: 311–325.

Meng, R., J. Wu, F. Zhao, B. D. Cook, R. P. Hanavan, and S. P. Serbin. 2018. "Measuring Short-Term Post-Fire Forest Recovery Across a Burn Severity Gradient in a Mixed Pine-Oak Forest Using Multi-Sensor Remote Sensing Techniques." *Remote Sensing of Environment* 210: 282–296.

Moreno-Mateos, D., A. Alberdi, E. Morriën, W. H. van der Putten, A. Rodríguez-Uña, and D. Montoya. 2020. "The Long-Term Restoration of Ecosystem Complexity." *Nature Ecology & Evolution* 4, no. 5: 676–685.

Muñoz-Sabater, J., E. Dutra, A. Agustí-Panareda, et al. 2021. "ERA5-Land: A State-of-the-Art Global Reanalysis Dataset for Land Applications." *Earth System Science Data* 13, no. 9: 4349–4383.

Nolan, R. H., L. Collins, A. Leigh, et al. 2021. "Limits to Post-Fire Vegetation Recovery Under Climate Change." *Plant, Cell & Environment* 44, no. 11: 3471–3489.

Olson, D. M., E. Dinerstein, E. D. Wikramanayake, et al. 2001. "Terrestrial Ecoregions of the World: A New Map of Life on Earth: A New Global Map of Terrestrial Ecoregions Provides an Innovative Tool for Conserving Biodiversity." *BioScience* 51, no. 11: 933–938.

Parks, S. A., C. Miller, C. R. Nelson, and Z. A. Holden. 2014. "Previous Fires Moderate Burn Severity of Subsequent Wildland Fires in Two Large Western US Wilderness Areas." *Ecosystems* 17: 29–42.

Pausas, J. G. 2015. "Bark Thickness and Fire Regime." *Functional Ecology* 29, no. 3: 315–327.

Pausas, J. G., and J. E. Keeley. 2009. "A Burning Story: The Role of Fire in the History of Life." *BioScience* 59, no. 7: 593–601.

Pausas, J. G., and J. E. Keeley. 2021. "Wildfires and Global Change." *Frontiers in Ecology and the Environment* 19, no. 7: 387–395.

Pérez-Cabello, F., R. Montorio, and D. B. Alves. 2021. "Remote Sensing Techniques to Assess Post-Fire Vegetation Recovery." *Current Opinion in Environmental Science & Health* 21: 100251.

Qin, Y., X. Xiao, J. P. Wigneron, et al. 2022. "Large Loss and Rapid Recovery of Vegetation Cover and Aboveground Biomass Over Forest Areas in Australia During 2019–2020." *Remote Sensing of Environment* 278: 113087.

Ramos, A. M., A. Russo, C. C. DaCamara, et al. 2023. "The Compound Event That Triggered the Destructive Fires of October 2017 in Portugal." *iScience* 26, no. 3: 106141.

Rifai, S. W., M. G. De Kauwe, R. V. Gallagher, L. A. Cernusak, P. Meir, and A. J. Pitman. 2024. "Burn Severity and Post-Fireweather Are Key to Predicting Time-to-Recover From Australian Forest Fires." *Earth's Futures* 12: e2023EF003780.

Roberts, D. A., P. E. Dennison, M. E. Gardner, Y. Hetzel, S. L. Ustin, and C. T. Lee. 2003. "Evaluation of the Potential of Hyperion for Fire Danger Assessment by Comparison to the Airborne Visible/Infrared Imaging Spectrometer." *IEEE Transactions on Geoscience and Remote Sensing* 41, no. 6: 1297–1310.

Rodman, K. C., T. T. Veblen, M. A. Battaglia, et al. 2020. "A Changing Climate Is Snuffing Out Post-Fire Recovery in Montane Forests." *Global Ecology and Biogeography* 29, no. 11: 2039–2051.

Rodrigues, M., À. C. Camprubí, R. Balaguer-Romano, et al. 2023. "Drivers and Implications of the Extreme 2022 Wildfire Season in Southwest Europe." *Science of the Total Environment* 859: 160320.

Rodrigues, M., J. de la Riva, D. Domingo, et al. 2024. "An Empirical Assessment of the Potential of Post-Fire Recovery of Tree-Forest Communities in Mediterranean Environments." *Forest Ecology and Management* 552: 121587.

Salesa, D., M. J. Baeza, E. Pérez-Ferrándiz, and V. M. Santana. 2022. "Longer Summer Seasons After Fire Induce Permanent Drought Legacy Effects on Mediterranean Plant Communities Dominated by Obligate Seeders." *Science of the Total Environment* 822: 153655.

Scholten, R. C., R. Jandt, E. A. Miller, B. M. Rogers, and S. Veraverbeke. 2021. "Overwintering Fires in Boreal Forests." *Nature* 593, no. 7859: 399–404.

Seidl, R., and M. G. Turner. 2022. "Post-Disturbance Reorganization of Forest Ecosystems in a Changing World." *Proceedings of the National Academy of Sciences of the United States of America* 119, no. 28: e2202190119.

Steel, Z. L., D. Foster, M. Coppoletta, et al. 2021. "Ecological Resilience and Vegetation Transition in the Face of Two Successive Large Wildfires." *Journal of Ecology* 109, no. 9: 3340–3355.

Stöckli, R., and P. L. Vidale. 2004. "European Plant Phenology and Climate as Seen in a 20-Year AVHRR Land-Surface Parameter Dataset." *International Journal of Remote Sensing* 25, no. 17: 3303–3330.

Turco, M., S. Jerez, S. Augusto, et al. 2019. "Climate Drivers of the 2017 Devastating Fires in Portugal." *Scientific Reports* 9, no. 1: 13886.

Veraverbeke, S., I. Gitas, T. Katagis, A. Polychronaki, B. Somers, and R. Goossens. 2012. "Assessing Post-Fire Vegetation Recovery Using Red–Near Infrared Vegetation Indices: Accounting for Background and Vegetation Variability." *ISPRS Journal of Photogrammetry and Remote Sensing* 68: 28–39.

Vermote, E. F., N. Z. El Saleous, and C. O. Justice. 2002. "Atmospheric Correction of MODIS Data in the Visible to Middle Infrared: First Results." *Remote Sensing of Environment* 83: 97–111.

Viana-Soto, A., I. Aguado, and S. Martínez. 2017. "Assessment of Post-Fire Vegetation Recovery Using Fire Severity and Geographical Data in the Mediterranean Region (Spain)." *Environments* 4, no. 4: 90.

Viana-Soto, A., I. Aguado, J. Salas, and M. García. 2020. "Identifying Post-Fire Recovery Trajectories and Driving Factors Using Landsat Time Series in Fire-Prone Mediterranean Pine Forests." *Remote Sensing* 12, no. 9: 1499.

Vicente-Serrano, S. M. 2006. "Evaluating the Impact of Drought Using Remote Sensing in a Mediterranean, Semi-Arid Region." *Natural Hazards* 40: 173–208.

Vieira, D. C. S., P. Borrelli, D. Jahanianfard, A. Benali, S. Scarpa, and P. Panagos. 2023. "Wildfires in Europe: Burned Soils Require Attention." *Environmental Research* 217: 114936.

Vogel, J., E. Paton, V. Aich, and A. Bronstert. 2021. "Increasing Compound Warm Spells and Droughts in the Mediterranean Basin." *Weather and Climate Extremes* 32: 100312.

Wittenberg, L., D. Malkinson, O. Beeri, A. Halutzy, and N. Tesler. 2007. "Spatial and Temporal Patterns of Vegetation Recovery Following Sequences of Forest Fires in a Mediterranean Landscape, Mt. Carmel Israel." *Catena* 71, no. 1: 76–83.

Xu, X., G. Zhou, H. Du, et al. 2020. "Combined MODIS Land Surface Temperature and Greenness Data for Modeling Vegetation Phenology, Physiology, and Gross Primary Production in Terrestrial Ecosystems." *Science of the Total Environment* 726: 137948.

Zhu, Z., S. Piao, R. B. Myneni, et al. 2016. "Greening of the Earth and Its Drivers." *Nature Climate Change* 6, no. 8: 791–795.

Zscheischler, J., S. Westra, B. J. Van Den Hurk, et al. 2018. "Future Climate Risk From Compound Events." *Nature Climate Change* 8, no. 6: 469–477.

Supporting Information

Additional supporting information can be found online in the Supporting Information section.